ACI STRUCTURAL JOURNAL TECHNICAL PAPER

Title No. 120-S58

Behavior of Unbonded Post-Tensioned Concrete Slabs Exposed to Fire

by Siyoung Park and Thomas H.-K. Kang

With the development and commercialization of post-tensioned (PT) concrete structures, concerns pertaining to structural safety for disasters and diverse conditions, such as fire and high temperatures, have emerged. To better understand fire-resistance performance, effects associated with cover thickness and tendon configurations for six unbonded PT concrete slabs were evaluated in regard to temperature changes, deflection, tendon tensile forces, and fire endurance/time. In addition, the factors and relationship between the extent of damage caused by concrete cracking/delamination and tendon force at post-tensioning were evaluated. Thermal resistance and deflection rates for materials such as galvanized steel duct or high-density polyethylene (HDPE) sheathing were also examined. It is the authors' hope that the aforementioned information identifying parameters affecting fire-resistance performance of PT slabs may be helpful to the practitioner when considering tendon configurations for unbonded PT concrete structures.

Keywords: cover thickness; fire-resistance performance; tendon configuration; unbonded post-tensioned (PT) slab.

INTRODUCTION

Since the introduction of post-tensioned (PT) systems in the United States in 1949,[1] the systems have been widely accepted in use for structures such as bridges, nuclear containment, water reservoirs/tanks, and buildings. Use of PT concrete systems permits the introduction of longer spans, slender members, effective crack control, and deflection mitigation.[2] With the introduction of PT systems, various tendon configurations, which are classified based on the type of strand(s), filling material(s), presence of duct, and anchorage components, were also introduced.[3-5] Among the diverse tendon configurations, this study focused on three types: unbonded bare-strand tendon (U), grouted extruded-strand tendon (G), and unbonded single-strand tendon (S). Characteristics of these three tendon configurations analyzed are summarized in Table 1.

The U-type is comprised of a galvanized steel duct and seven-wire strands with grease coating (also known as PT coating), which were obtained from high-density polyethylene (HDPE)-sheathed single-strand tendons with the HDPE sheath removed. On the other hand, the G-type encompasses the use of galvanized steel duct, cement grout, and HDPE-sheathed single-strand tendons. The S-type has only the HDPE-sheathed single-strand tendons (without the galvanized steel duct and cement grout).

Grease in the tendon is used to prevent corrosion and keep the strands unbonded. Although HDPE encasement increases duct size and yields more difficult strand installation, it is used in G-type installation due to the benefits fixed to the lift-off procedure and individual strand replacement. Removal of the duct in the S-type configuration, which is typical for building structures, simplifies the process of tendon placement.[3-6]

Despite the advantages of unbonded PT systems, their vulnerability at elevated temperatures is frequently questioned. At elevated temperatures, degraded strength and stiffness of the various structural materials employed have detrimental effects on the overall structural performance[7-14] (Fig. 1).

PT members are more susceptible to fire than reinforced concrete (RC) structures for the following reasons[2,15-18]: 1) use of higher-strength concrete resulting in greater likelihood of potential concrete spalling; 2) higher effective stress of tendons resulting in greater likelihood of potential steel fracture; and 3) tension force demand imposed on each strand is higher than that on each reinforcing bar for the same number (so risk of fire damage to the structure is greater). As a result, prescriptive design codes[19,20] (Tables 2 and 3) and safety design manual/codes[12-14] have been enacted following the concept of fire-safety engineering to reduce and prevent potential fire accidents.[21]

Few studies exist that were conducted to evaluate the fire-resistance performance of PT concrete structures. Bailey and Ellobody[22,23] conducted fire tests on both bonded and unbonded PT one-way concrete slabs to understand the basic fire performance of structures for plastic and metallic ducts, limestone and Thames gravel aggregates, and longitudinal constraint conditions. Gales et al.[24] illustrated the response of a continuous unbonded PT concrete structure under localized transient heating. Initial prestresses for the test specimens in the study were set at 917 to 1036 MPa (132 to 149 ksi), which corresponds to 52 and 55% of the tendon's ultimate strength, respectively. The variables were: the temperature increase rate at 2.0, 10.0, and 30.0°C (3.6, 18.0, and 54.0°F); the target soak temperature (200 to 700°C [392 to 1292°F]); and soaking time (5, 45, and 90 minutes). The heating length ratio effects on prestress relaxation at the ramp and cool stages were evaluated by comparing test data from MacLean.[25] Creep deformation was found prominent between 300 and 400°C (572 and 752°F), with a drastic decrease in tendon stress at temperatures above

ACI Structural Journal, V. 120, No. 3, May 2023.
MS No. S-2022-223.R1, doi: 10.14359/51738512, received October 20, 2022, and reviewed under Institute publication policies.

Table 1—Characteristics of three tendon configurations (Shin et al.[3] and Park[5])

Type	Unbonded bare-strand tendon (U)	Grouted extruded-strand tendon (G)	Unbonded single-strand tendon (S)
Composition, mm	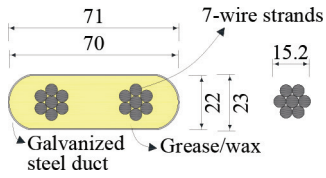	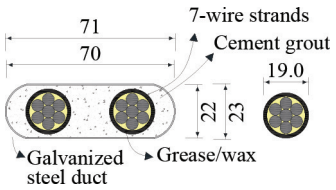	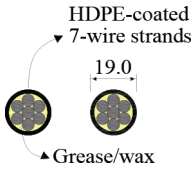
Adverse effects	Leakage of flexible fillers	HDPE sheath damage	HDPE sheath damage
Strand installation	Easy	Difficult	Difficult
Duct size	Small	Large	—
Detensioning	Possible but difficult	Possible and easy	Possible and easy
Restressing			
Replacement of strands			
Stress measurement of tendon in service	Possible	Possible	Possible
Stress measurement of individual strand in service	Impossible	Possible	Possible

Note: 1 mm = 0.0394 in.

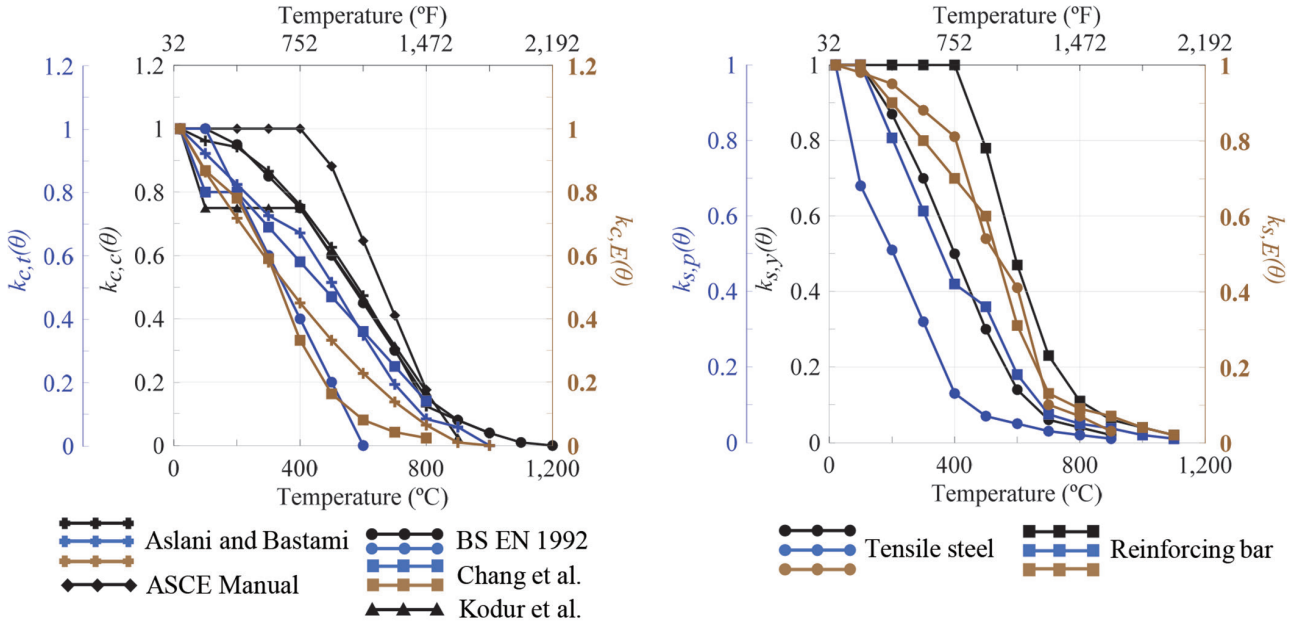

(a) Concrete (ASCE Manual,[12] Aslani and Bastami,[7] BS EN 1992-1-2,[13] Chang et al.,[8] and Kodur et al.[9])

(b) Steel (BS EN 1992-1-2[13])

Fig. 1—Material properties degradation at elevated temperatures.

300°C (572°F). Hou et al.[26] also tested unbonded PT slabs for variables associated with cover thickness, load level, and degree of prestressing. The ability to sustain the elastic modulus of the tendon was found to increase with significant increase in cover thickness. With an increase in the degree of prestressing, concrete members were found to have higher susceptibility to spalling.

Numerical analyses were also performed to assess the behavior of RC slabs under static and fire loads. Wosatko et al.[27] and Genikomsou and Polak[28] analyzed the punching shear behavior of an RC slab with a three-dimensional (3-D) finite element model. The damaged plasticity model of concrete was calibrated, and the shear behavior and crack patterns of the RC slab were presented as the result of analysis. Al Hamd et al.[29] introduced the load-induced thermal strain of the flat slab. Modeling of fire and thermal expansion of the slab was studied, evaluating the punching shear strength. Kodur and Bhatt[30] modeled fiber-reinforced polymer-strengthened concrete slabs numerically and presented the thermomechanical response of the slabs.

Karaki et al.[31] assessed the thermal response of slabs by using the probabilistic method. The analysis for general thermal-related factors such as conductivity, specific heat, and so on was performed, and validated by sensitivity analysis.

To improve the fire resistance of structures, codification based on performance-based design (PBD) research is relatively recent. The concept of PBD was introduced in the New Zealand Building Code[32] in the form of hierarchical provisions for structural stability. In Yang et al.,[33] the roadmap and vision for PBD for fire were discussed, and the American Society of Civil Engineers/Structural Engineering Institute (ASCE/SEI)[34] demonstrated proper execution of performance-based structural fire design (PBSFD) in accordance with ASCE 7-16, Appendix E, while providing procedural guidance. For the application of PBD, research based on experimental and numerical methods has progressed. Dai et al.[35] reviewed travelling fire[36] scenarios, and Jeanneret et al.[37] derived acceptance criteria for unbonded PT concrete subject to improved travelling fire[38] in terms of thermal boundaries.

For this study, test parameters included cover thickness, slab thickness, and tendon configuration. The temperature, deflection, and tensile force were measured on specimens subjected to sustained vertical load and monotonically increasing heat.

RESEARCH SIGNIFICANCE

ACI/TMS 216.1-14[19] (or the 2018 International Building Code [IBC][20]) specifies prescriptive fire safety design codes but does not incorporate specific provisions. Due to experimental site condition constraints and high cost, limited studies have been carried out. The purpose of this study is to determine the fire-resistance performance of unbonded PT one-way concrete slabs under three different tendon configurations. Additionally, the thermal effect on each tendon configuration was analyzed with the benefits introduced. Data and submitted analysis of the resulting fire tests are intended to be used to help improve prescriptive and PBD fire design codes.

Table 2—Prescriptive fire-resistance rating for thickness of concrete slab (ACI/TMS 216.1-14[19] and 2018 IBC[20])

Aggregate type	Minimum equivalent thickness for fire-resistance rating, mm (in.)				
	1 hour	1-1/2 hours	2 hours	3 hours	4 hours
Siliceous	88.9 (3.5)	109.2 (4.3)	127 (5.0)	157.5 (6.2)	177.8 (7.0)
Carbonate	81.3 (3.2)	101.6 (4.0)	116.8 (4.6)	144.8 (5.7)	167.6 (6.6)
Semi-lightweight	68.6 (2.7)	83.8 (3.3)	96.5 (3.8)	116.8 (4.6)	137.2 (5.4)
Lightweight	63.5 (2.5)	78.7 (3.1)	91.4 (3.6)	111.8 (4.4)	129.5 (5.1)

EXPERIMENTAL PROGRAM

General

For the experimental study, six unbonded PT slabs designed according to ACI 318-19,[39] ACI/TMS 216.1-14,[19] and ASTM E119-20[40] were tested. The PT concrete slab details are shown in Fig. 2. The tendon number and profile were determined using the load-balancing method.[41] The tendon number was that required to resist 160% of the self-weight of concrete, and the tensile force was 60% of its ultimate strength (153.4 kN [34.5 kip]) at the test date. The steel reinforcement (reinforcing bars and tendons) and layout for each slab were the same: eight 13.0 mm (0.5 in.) diameter longitudinal bars at the bottom, two 10.0 mm (0.4 in.) diameter longitudinal bars at the top, 10.0 mm (0.4 in.) diameter transverse bars at an interval of 275 mm (10.8 in.) placed along the bottom and top, and six seven-wire strands. For each U- and G-type specimen, three ducts were installed. Each duct contained two seven-wire strands. Extra transverse bars (six 10.0 mm [0.4 in.] diameter bars) and hairpin bars (six 10.0 mm [0.4 in.] diameter bars) were installed within the anchorage zone at both ends of the slab to withstand bursting or spalling stresses induced by post-tensioning.

The length and width for the slabs were identical: 6700 and 1500 mm (264.0 and 59.1 in.), respectively, whereas the height and cover thickness for each slab were designed based on the target fire-resistance rate. Corresponding to ACI/TMS 216.1-14[19] for unrestrained boundary conditions and siliceous aggregate type, 2- and 3-hour fire-resistance slabs were designed with a cover thickness of 45.0 and 60.0 mm (1.8 and 2.4 in.), respectively. With the designed cover thickness and tendon profile, the thickness of the slabs was set to be 250 and 280 mm (9.9 and 11.0 in.), respectively, satisfying the minimum slab equivalent thickness requirement of 125.4 and 157.5 mm (5.0 and 6.2 in.), respectively. Using the tendon configuration and cover thickness, the test slabs were named as PF-U45 (U-type, 45 mm [1.8 in.]), PF-U60 (U-type, 60 mm [2.4 in.]), PF-G45 (G-type, 45 mm [1.8 in.]), PF-G60 (G-type, 60 mm [2.4 in.]), PF-S45 (S-type, 45 mm [1.8 in.]), and PF-S60 (S-type, 60 mm [2.4 in.]).

Table 3—Prescriptive minimum cover for fire resistance (ACI/TMS 216.1-14[19] and 2018 IBC[20])

Aggregate type	Cover for corresponding fire resistance, mm (in.)					
	Restrained	Unrestrained				
	4 or less	1 hour	1-1/2 hours	2 hours	3 hours	4 hours
Siliceous	19.1 (3/4)	28.6 (1-1/8)	38.1 (1-1/2)	44.5 (1-3/4)	60.3 (2-3/8)	69.9 (2-3/4)
Carbonate	19.1 (3/4)	25.4 (1)	34.9 (1-3/8)	41.3 (1-5/8)	54.0 (2-1/8)	57.2 (2-1/4)
Semi-lightweight	19.1 (3/4)	25.4 (1)	34.9 (1-3/8)	38.1 (1-1/2)	50.8 (2)	57.2 (2-1/4)
Lightweight	19.1 (3/4)	25.4 (1)	34.9 (1-3/8)	38.1 (1-1/2)	50.8 (2)	57.2 (2-1/4)

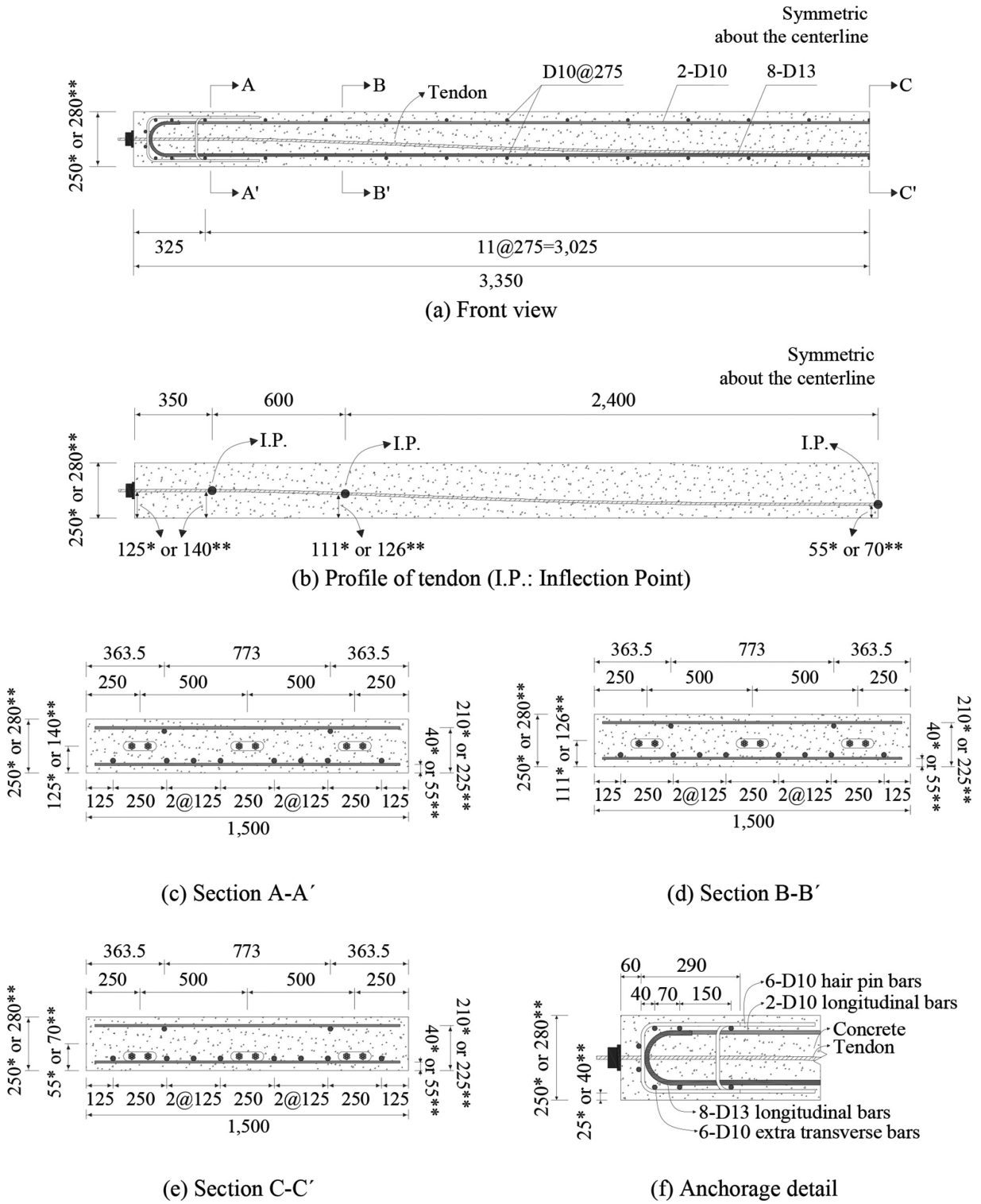

*Fig. 2—Details of PT concrete slabs (*indicates specimens with 45 mm cover thickness; and **indicates specimens with 60 mm cover thickness). (Note: Units in mm; 1 mm = 0.0394 in.)*

Material properties

The concrete cast throughout consisted of identical proportions. The proportions per 1 m^3 were as follows: cement (Type 1 portland), 468 kg (1029.6 lb); fine aggregate, 783 kg (1722.6 lb); coarse aggregate, 953 kg (2096.6 lb); high-range water-reduction agent, 4.8 kg (10.6 lb); and water, 165 kg (363.0 lb), with a water-cement ratio (*w*/*c*) of 35.3% and a slump of 150 mm (5.9 in.).

The design concrete compressive strength was 40.0 MPa (5.8 ksi). In Table 4, the compressive strength for each specimen conducted through the concrete cylinder test in accordance with ASTM C39/C39M-21[42] at jacking testing is shown.

KS D 3504 steel was used for reinforcing bars with a specified yield strength of 400 MPa (57.6 ksi), and KS D 7002 steel was used for the tendon strands. The tensile

Table 4—Results of concrete cylinder tests

Specimen	Type	Age, days	Compressive strength, MPa
PF-U45	Jacking	20	40.2
	Testing	35	46.7
PF-U60	Jacking	20	40.2
	Testing	48	49.5
PF-G45	Jacking	16	46.0
	Testing	29	49.1
PF-G60	Jacking	16	46.0
	Testing	45	47.6
PF-S45	Jacking	14	30.0
	Testing	33	36.5
PF-S60	Jacking	14	30.0
	Testing	47	38.2

Note: 1 MPa = 0.144 ksi.

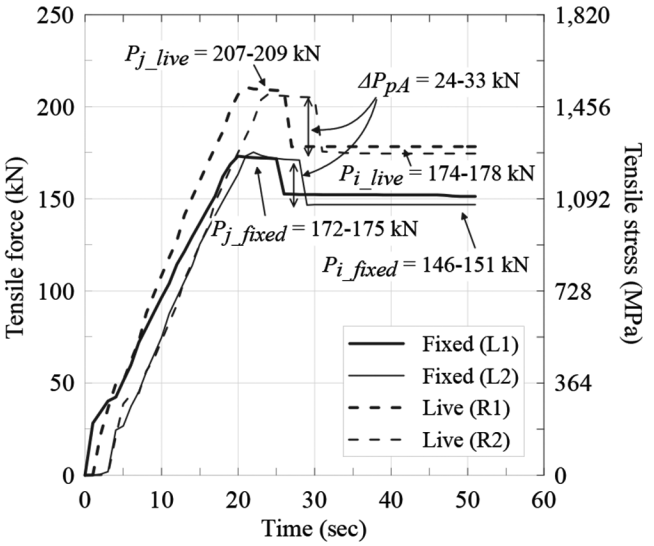

Fig. 3—Jacking force data of PF-U45. (Note: 1 kN = 0.2247 kip; 1 MPa = 0.144 ksi.)

(a) Furnace, actuator, and insulated covers

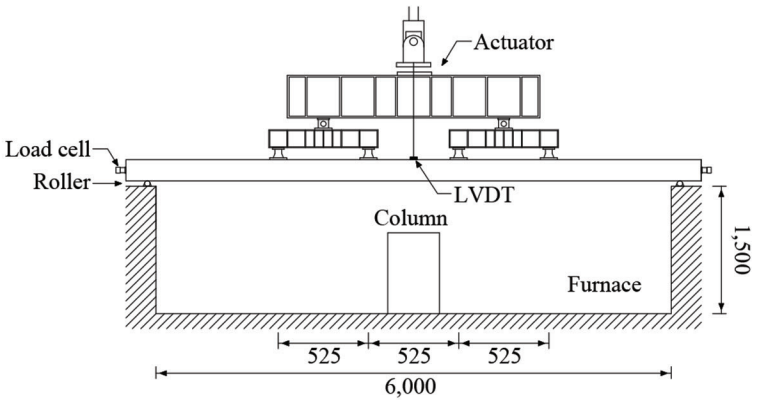

(b) Front view (unit: mm). (Note: 1 mm = 0.0394 in.)

Fig. 4—Fire test settings.

strength test conducted on the tendon stands yielded values for measured yield strength, ultimate strength, and elastic modulus of 1670, 1896, and 200,000 MPa (240.5, 273.0, and 28,800 ksi), respectively.

Post-tensioning

Jacking forces were applied to the tendons in each slab 14 to 20 days after concrete placement. The concrete compressive strength for each specimen at the jacking date is shown in Table 4. The jacking forces applied used a hydraulic single-strand jack with a target force of 200 kN (44.9 kip). Loading was continuously recorded using self-made load cells. Representative jacking force data for PF-U45 are shown in Fig. 3. Jacking operations for each specimen followed the same procedure, whereby the tendons were jacked at the live end with the other fixed. After jacking to 200 kN (44.9 kip), anchorage slip resulted in tensile force loss of 30.0 to 40.0 kN (6.7 to 9.0 kip), correspondingly 12 to 16% of the ultimate strength. At the time of testing, the effective tensile force measured was approximately 160 kN (36.0 kip) at the live end and 135 kN (30.3 kip) at the fixed end.

Test setup and instrumentation plan

Figure 4 shows the fire test settings. The dimensions of the furnace were 6000 x 2400 x 1500 mm (236.4 x 94.6 x 59.1 in.). An internal column was located inside the furnace to protect it should the slab test specimen rupture. The slab specimens were simply supported on two transverse cylindrical rods, having a span length of 6200 mm (244.3 in.). Insulated covers were installed on both sides of the specimens to prevent temperature loss due to heat transfer between the furnace and the air and to preserve the furnace's internal pressure. Sustained vertical loading was applied to each slab using a hydraulic jack, spreader beam, and four loading plates. A total force of 120 kN (27.0 kip), including the self-weight of the actuator, was applied to the slab. Said load corresponds to 40 and 37.5% of the moment capacity of the slabs having a thickness of 250 and 280 mm (9.9 and 11.0 in.), respectively. The furnace temperature followed the ISO 834-1:1999[43] time-temperature curve.

A wire linear variable displacement transducer (LVDT) was installed at the center of the slab to monitor the deflection of the slab during the fire tests. Self-made load cells were installed at anchorage points, as shown in Fig. 4(a).

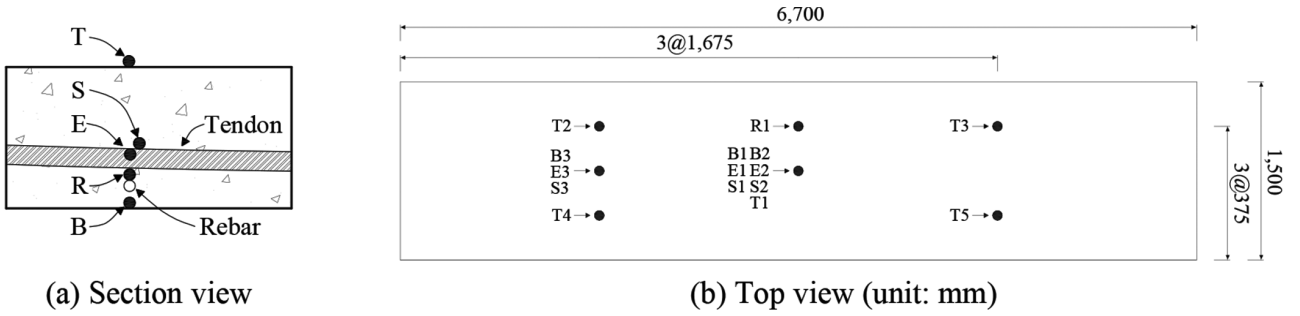

Fig. 5—Location details and notations of thermocouples. (Note: 1 mm = 0.0394 in.)

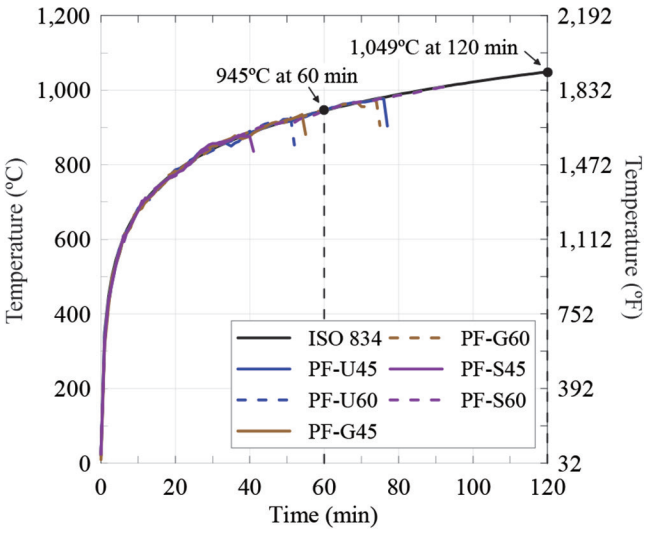

Fig. 6—Measured furnace temperatures during fire tests.

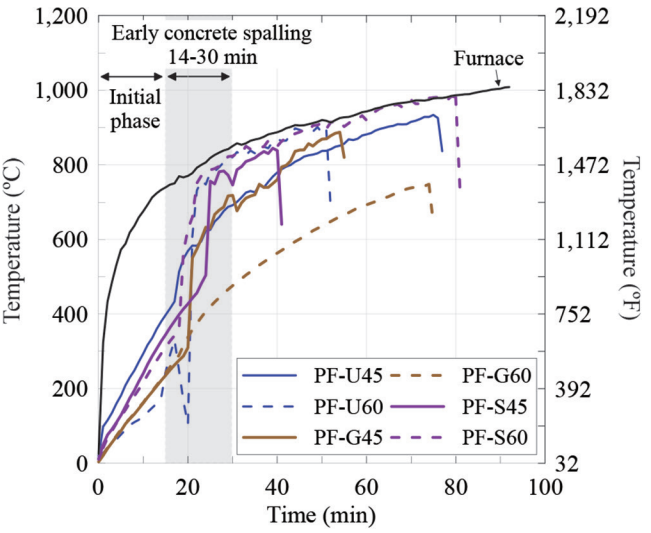

Fig. 7—Time-temperature curves at bottom of slabs.

The differences in tendon tensile force at the fixed and live ends were measured and compared during the fire tests. Fifteen thermocouples, corresponding to the locations and labels shown in Fig. 5, were installed in each slab. From start to end, temperature variations during the fire tests were measured at the bottom and top of the slab, tendons, reinforcing bars, and ducts. The furnace itself was equipped with thermocouples to monitor the temperature of the monotonically (strictly) increasing heat. Figure 6 shows the measured furnace temperatures during the fire tests.

Fire resistance and failure criteria

The fire resistance of the slabs was evaluated based on the criteria specified in ASTM E119-20. The critical temperature for cold-drawn prestressing steel and reinforcing steel is specified as 427 and 593°C (800 and 1100°F), respectively. In terms of deflection and deflection rate, the conditions of acceptance are specified as $L_c^2/(400d)$ and $L_c^2/(9000d)$ for the maximum total deflection and the maximum deflection rate per minute, respectively, where L_c is the clear span of the beam, and d is the distance between the extreme fiber of the beam in the compression zone and the extreme fiber of the beam in the tensile zone.

FIRE TEST RESULTS AND DISCUSSION

Thermal response of PT concrete slabs

Figure 7 shows the time-temperature curves at the bottom of the slabs. During the initial phase, the bottom temperature steadily increased in all the specimens, followed by a period of temperature fluctuation. According to previous studies,[15-18] the temperature fluctuating period is indicative of early concrete spalling (that is, concrete breaks down near the fire-damaged surface). Early concrete spalling occurred between 14 and 30 minutes after the fire test began. With the temperature increase, temperature rates stabilized after passing through the early concrete spalling period. The depth of spalling and potential induced damage during the fire test was restricted with the placement of bottom reinforcing bars. Otherwise, concrete spalling, which results in section area loss, would have weakened the fire-resistance performance due to heat penetration to the tendons.

Figure 8 shows the variation of the temperature at the tendon with respect to time. In general, four distinct stages were observed: 1) the initial plateau stage; 2) the rapid temperature increase stage; 3) the second plateau stage; and 4) the gradual temperature increase stage. The second plateau stage appears to be influenced by the evaporation of free water in the concrete and occurred when tendon temperatures neared 100°C (212°F).

The tendon configuration and cover thickness also had an effect on the temperature rate increase at each step. For cover thickness of 45 mm (1.8 in.), PF-S45 experienced a rapid temperature increase from initiation of the fire test and earliest termination, 40 minutes. Previous studies[16,17] indicated that fire damage is amplified when a sudden increase in temperature occurs at the tendon. When cover thickness

was increased from 45 to 60 mm (1.8 to 2.4 in.), the duration of the fire test for PF-S60 was expanded to 90 minutes (125% increase in duration compared to PF-S45). The effect of cover increase was also seen for the G-type tendons, to which fire endurance improved from 55 to 75 minutes (36% increase).

The U-type tendons experienced a decrease in fire endurance time from 77 to 52 minutes (32% decrease). Said adverse effect was observed in the pattern of the deflection rate for PF-U60, where the fire-resistance performance was influenced by concrete delamination or blowout. For U-type tendons, grease was lubricated on the surface of the strands (that is, PT coating), leaving most of the duct area air. After tensioning, strands might have been attached to the top of the duct at the middle region and the bottom of the duct at the support region, with strands not touching the inner duct in between them. During fire tests, this would have applied much more locally concentrated force from the tendon to the concrete than the G- and S-types enclosed by grout (G-type) or concrete (S-type). The force might have been distributed more evenly in the G- and S-types. Speculation is that, with larger and heavier concrete cover at the middle region, localized splitting of the concrete along the tendon and the tensile fracture of the bottom concrete occurred earlier in PF-U60 than PF-U45.

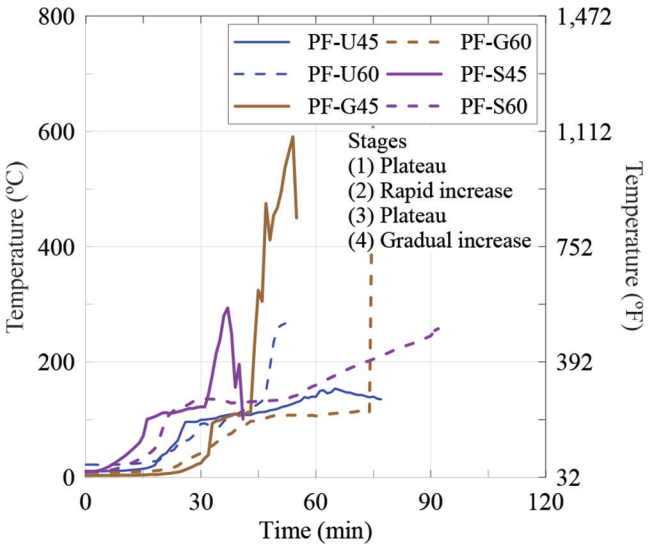

Fig. 8—Time-temperature curves at tendons.

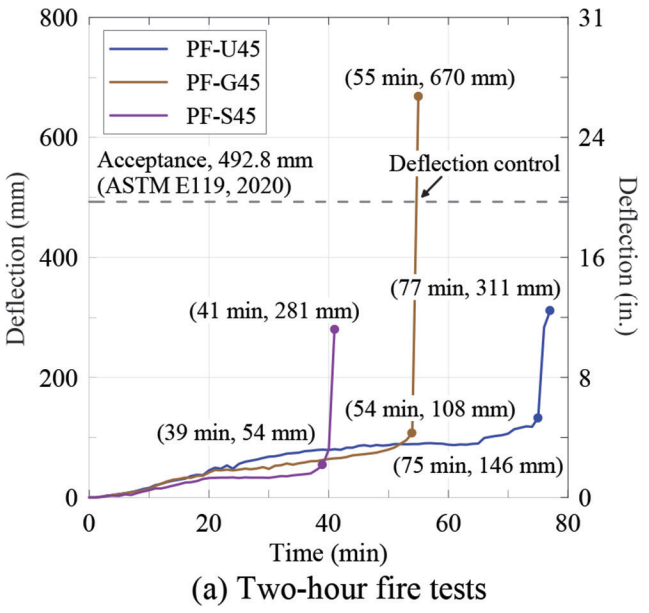

Fig. 9—Time-deflection curves at midspan of slabs.

Flexural response of PT concrete slabs

Figure 9 shows the measured midspan deflection of each slab. The fire tests were terminated when deflection exceeded the acceptance criteria specified in ASTM E119,[40] and the slabs were considered to have lost their structural capacity. In the initial phase, the deflection of all slabs gradually increased with time at similar rates given they were manufactured to have similar flexural capacities regardless of tendon configuration.

However, the time of failure varied with the tendon configuration. For slab thicknesses of 250 mm (9.9 in.), deflections just prior to the slab rupture were 146, 108, and 54.0 mm (5.5, 4.3, and 2.1 in.) for PF-U45, PF-G45, and PF-S45, respectively. With an increase in slab thickness to 280 mm (11.0 in.), deflection immediately before slab rupture changed to 88.0, 134, and 160 mm (3.5, 5.3, and 6.3 in.) for PF-U60, PF-G60, and PF-S60, respectively. The maximum deflection of PF-U60 decreased by 39.7% when compared to PF-U45, whereas the maximum deflection of PF-G60 increased by 24.1% when compared to PF-G45, and PF-S60 increased by 196.3% when compared to PF-S45.

Increased cover thickness resulted in similar change rates on the fire endurance time and maximum deflection just prior to slab rupture for all tendon configurations.

Figure 10 shows the relationship between tendon temperature and deflection. At the initial stage, the tendon temperature remained constant, except for S-type tendon configurations with deflection increase attributed to concrete stiffness degradation caused by elevated temperatures in the slabs' bottom layer. With the increase in temperature, stiffness

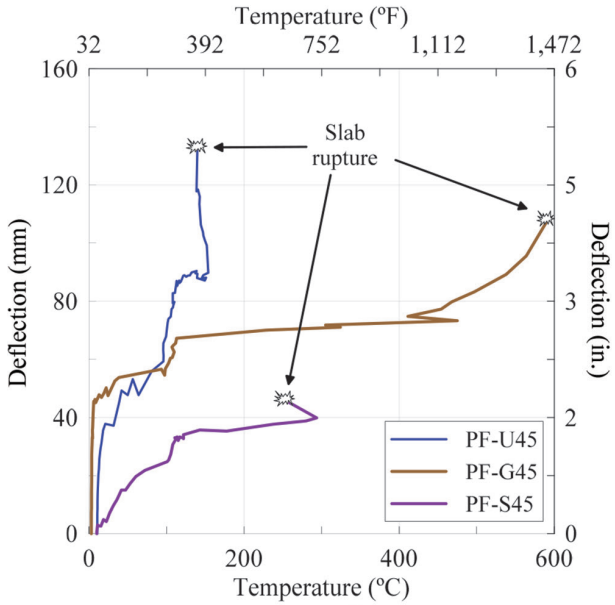

(a) Two-hour fire tests

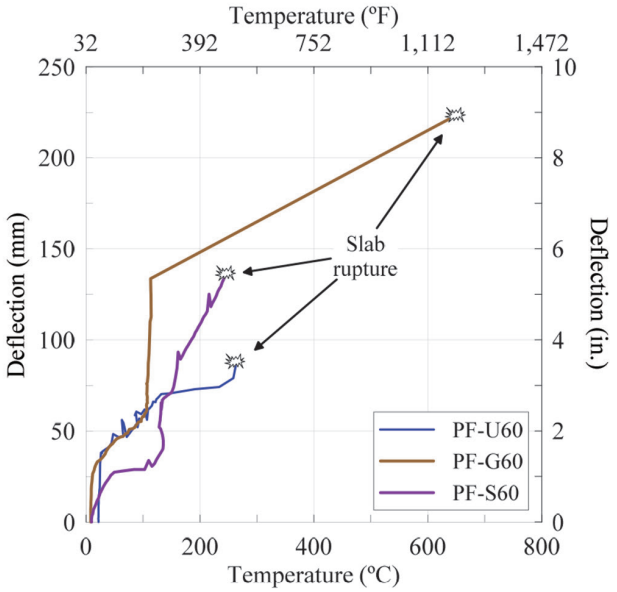

(b) Three-hour fire tests

Fig. 10—Tendon temperature-deflection curves during fire tests.

degradation of both the concrete and tendon resulted in an increase in deflection until the slabs ruptured. The measured peak tendon temperatures for PF-U45, PF-U60, PF-G45, PF-G60, PF-S45, and PF-S60 were 155, 265, 590, 650, 290, and 250°C (311, 509, 1094, 1202, 554, and 482°F), respectively. The acceptance temperature of tension steel in fire tests specified by ASTM E119[40] is 427°C (800°F). The peak tendon temperatures for G-type tendons were exceeded, whereas those for U-type and S-type tendons were not. The peak temperatures of PF-U45, PF-U60, PF-S45, and PF-S60 were 36, 62, 68, and 59% lower than the critical temperature identified. Thus, early termination of fire tests was not attributed to tendon rupture associated with increased temperature but that of other factors such as sustained loading, excessive deflection, and concrete delamination.

Tendon force variation during fire tests

The variation of tensile force in each tendon configuration is shown in Fig. 11. Consistent patterns were found in all tendon configurations: 1) the tensile force increasing stage; 2) the tensile force decreasing stage; and 3) the rupture stage.

In the first stage (30 to 40 minutes into fire exposure), the tensile force of the tendon gradually increased with time from 10 to 20 kN (2.2 to 4.5 kip). During this period, the tendon temperature shown in Fig. 8 reaches 100°C (212°F). Per Eurocode 2,[13] the degradation of mechanical properties of concrete and steel for elastic modulus and strength is negligible between 0 to 100°C (32 to 212°F). Thus, the increase in tensile force of the tendons in the first stage may be attributed to the gradual increase in deflection shown in Fig. 10, rather than property degradation.

During the second stage (that is, the tensile force decreasing stage), tensile forces returned to their original effective tensile force (10 to 20 kN [2.2 to 4.5 kip] decrease from the peak forces). Deflection increased similarly as in the first stage, but the tendon temperature rose above 100°C (212°F), reaching 200 to 300°C (392 to 572°F). At a temperature of 300°C (572°F), a 12% decrease in elastic modulus along with a 30% decrease in tendon yield strength and a 68% decrease in its proportional limit reference Eurocode 2.[13] Combined, said tendon mechanical degradations and the heat-induced elongations may have led to decreased tensile force.

The third stage was the period linked to rapid change in the tensile force and slab rupture. The deflection of the slabs rapidly increased as a result of the tendons being directly exposed to fire due to concrete delamination (blowout) and the accompanying fracture of the tendon near the support (Fig. 12) or failure to sustain imposed loading due to mechanical degradation.

Cracking and delamination of PT concrete slabs

Regional spalling at the bottom surface of the slabs and concrete delamination (blowout) at support regions near the anchor were observed in all the specimens during the fire tests. Figure 13 shows the observed cracks (thermal shrinkage crack, flexural crack, and delamination crack) for the PF-U45 specimen. The PF-U45 case well presents crack propagation and/or concrete delamination along the support and middle regions, making it suitable for analyzing the specimen. Propagation, channelization, and growth of thermal shrinkage cracks in regions are attributed to free water in the concrete specimens evaporating during the fire tests. Flexural cracks, propagated by sustained vertical loads and mechanical property (strength and stiffness) degradation due to fire, were observed from the center to the quarter regions at the top surface and bottom layer. These flexural cracks, combined with thermal shrinkage cracks, became a passageway for heat penetration into the tendon and duct. Delamination cracks observed propagated near anchor regions. The premise is that increased tendon tensile force (Fig. 11) and degraded concrete tensile strength due to elevated temperatures affected delamination crack propagation.

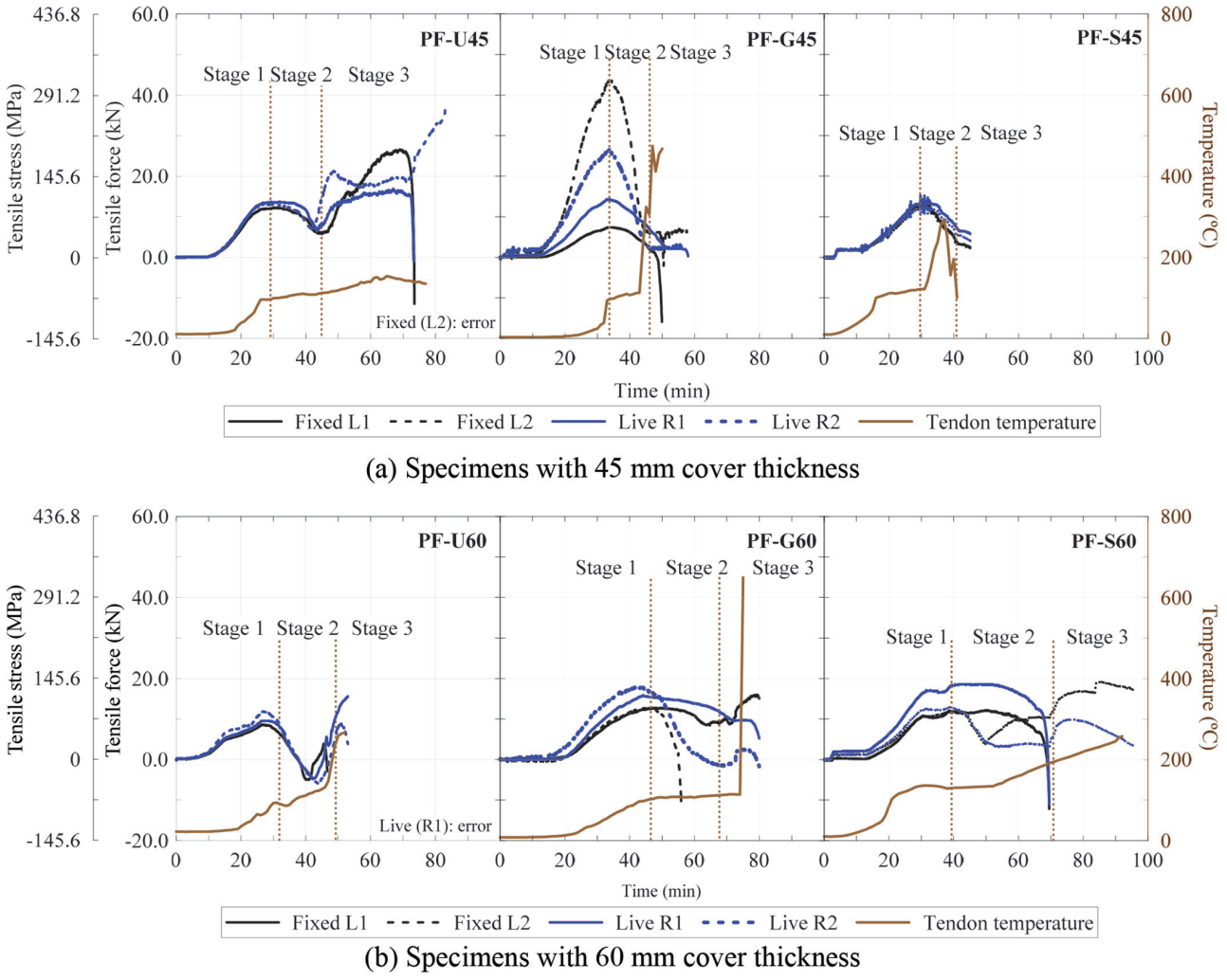

Fig. 11—Variation of tensile force in each tendon configuration. (Note: 1 mm = 0.0394 in.; 1 kN = 0.2247 kip; 1 MPa = 0.144 ksi; °F = 1.8 × °C + 32.)

Figure 14 shows the damage and degree of concrete cracks, spalling, and delamination (blowout) of the PF-U45 specimen, as well as suspect factors influencing the occurrence of concrete delamination at support regions. In Fig. 14, the concrete spalling damage shown, with the exception of anchorage zones, was limited by the use of bottom reinforcing bars having a cover thickness of 45 to 60 mm (1.8 to 2.4 in.). Delamination within support regions reached damaged depths of 130 to 260 mm (5.1 to 10.2 in.). In Fig. 14(a), the live end (left) suffered 19% greater damage (depth) than the fixed end (right).

The premise is that the tendon profile and applied tensile force had an effect on concrete delamination. Figure 14(c) shows the effective tensile force (P_e) along the length of the tendon before the test, as computed in accordance with ACI 423.10R-16.[44] The tendon effective tensile forces were 160 and 135 kN (36.0 and 30.3 kip), respectively, with the live-end forces being 18.5% greater than the fixed-end forces. In addition, damage caused by concrete delamination differed according to the anchor conditions. In Fig. 2(b), the tendon profile was designed to be negative parabolic at anchor regions throughout 950 mm (37.4 in.) length of the slab. As a result, a downward force (bursting force) was applied to the concrete, as shown in Fig. 14(b). Additionally, the tensile forces exceeded the initial force applied during fire testing (Fig. 11), resulting in increased bursting force and blowout (that is, delamination) of concrete below the tendon.

In total, tensile strength degradation due to elevated temperatures and downward force caused by negative tendon curvature were considered as factors affecting concrete delamination.

It should be noted that fire tests conducted for this study were performed under more severe conditions than ASTM E119[40] minimum conditions, using 6700 mm (264.0 in.) long specimens subject to a heating length of 6000 mm (236.4 in.). A fire assessment under real-life conditions is required. For continuous unbonded PT structures, fire impacts over a limited area are anticipated to have less influence on deflection and elongation (that is, less strain increment) of the tendons. Additionally, redundancy of one- or two-way slabs and stress redistribution within multiple tendons after minor tendons are damaged by fire in multi-span buildings should also be considered. These factors combined can help prevent concrete delamination and collapse of the structure.

EFFECTS OF THERMAL CONDUCTION AND DEFLECTION RATE

Thermal conduction

The effect of galvanized steel ducts in PT concrete structures was influential in terms of thermal conduction. As shown in Fig. 8, the time at which tendon temperature increased varied by tendon configuration, with the S-type experiencing the earliest temperature increase. According to previous studies,[45-47] thermal resistance occurs at the interface of two materials where voids and fluids exist that have lower thermal conductivity than solids (concrete and steel). This thermal resistance is explained by the concept of contact conductance (h_j), described in terms of Newton's law of cooling as Eq. (1)

$$q = h_j(\Delta T) \quad (1)$$

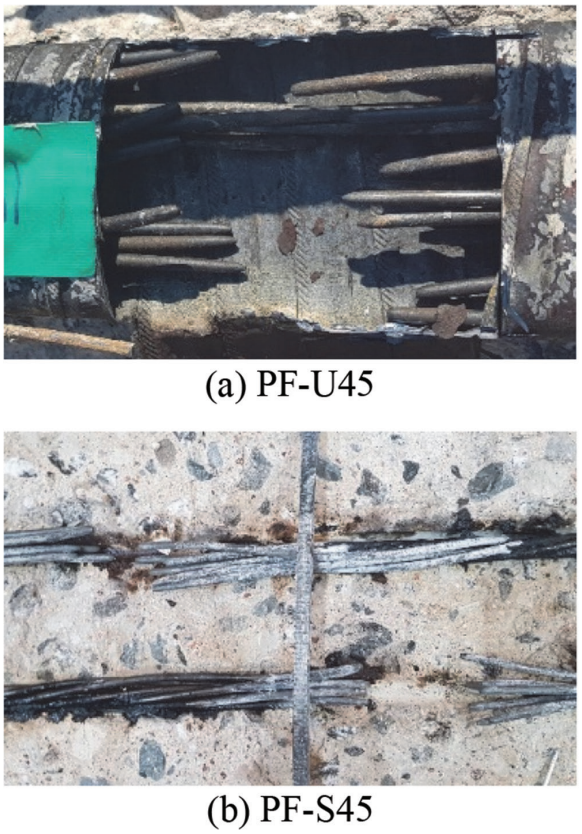

Fig. 12—Photographs of fractured tendons after fire tests.

where q is heat flux; h_j is thermal contact conductance; and ΔT is temperature drop across the interface. The S-type tended to gradually increase in temperature from the start (4 minutes after the fire test began), whereas the U-type started to increase in temperature 16 minutes after the fire test began, and the G-type started to increase 26 minutes after the fire test began.

The effect of HDPE sheathing on thermal resistance can also be evaluated by comparing the U- and G-types using the thermal contact conductance concept. HDPE sheathing of the G-type delayed the commencement of the increase in tendon temperature by 10 minutes compared to the U-type, despite the fact that grout (solid) composing the G-type has a higher thermal conductivity than air composing the U-type. This demonstrates the superior thermal flow resistance of HDPE sheathing. The tendon temperature of 100°C (212°F) is critical because it is the period when tensile force (tensile stress) stops increasing but starts decreasing, as shown in Fig. 12, implying degradation of mechanical properties of the tendon. Also, as shown in Fig. 1(b), tendon temperature escalation during fire is structurally detrimental. Thus, thermal resistance based on contact conductance should be considered when assessing the fire-resistance performance of PT concrete structures.

Deflection rate

Deflection rates were monitored to assess fire endurance due to unexpected or substantial deflection development during the fire test.[48] The deflection rates varied according to tendon configuration, with the resulting curves shown in Fig. 15. The deflection rates for PF-G45 and PF-S45 ranged from 2.5 to 5 mm/min (0.1 to 0.2 in./min), whereas PF-U45 ranged from 5 to 10 mm/min (0.2 to 0.4 in./min). With an increase in cover thickness, differences in deflection rate due to tendon configuration magnified. The deflection rates for PF-G60 and PF-S60 ranged from 0 to 2.5 mm/min (0 to 0.1 in./min), whereas PF-U60 ranged from 5 to 12 mm/min (0.2 to 0.5 in./min). Despite the few specimens exceeding acceptance criteria for tendon temperature just prior to slab rupture as specified in ASTM E119,[40] deflection rates for each test exceeded acceptance criteria. Thus, it may be considered the basis for judgment of structure failure.

Although the deflection rate was found to be a crucial factor in determining structure failure, HDPE coating had

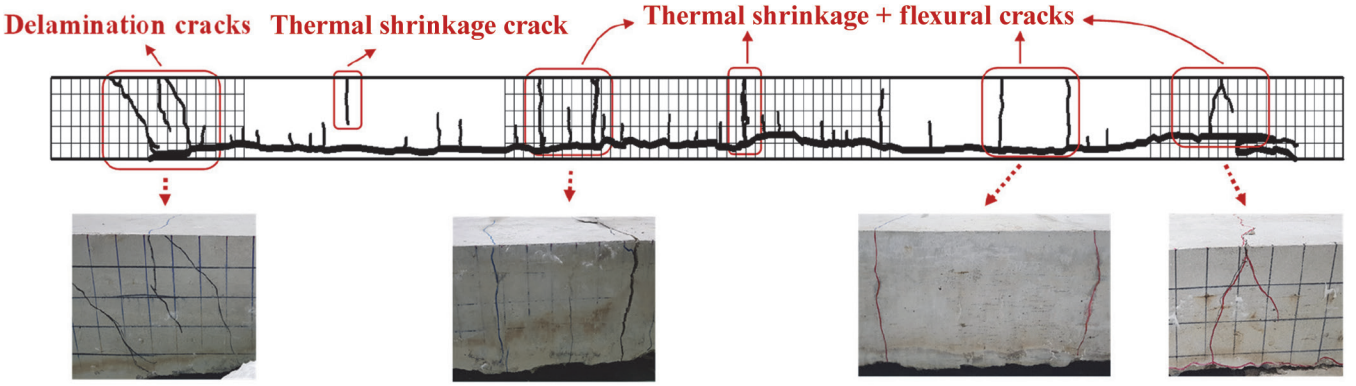

Fig. 13—Propagated cracks after fire test of PF-U45 specimen.

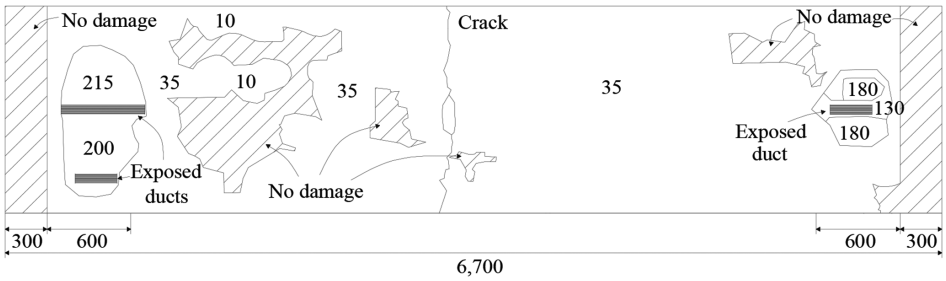

(a) Damage and degree of concrete cracks and delamination of PF-U45 specimen
(Number indicates depth of delamination and spalling; Unit: mm)

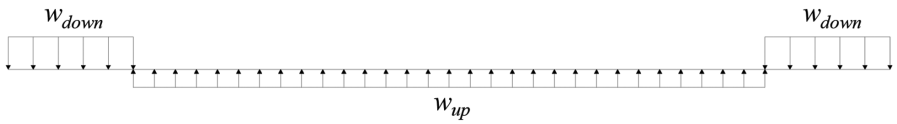

(b) Forces acting on concrete by tendon tensile force

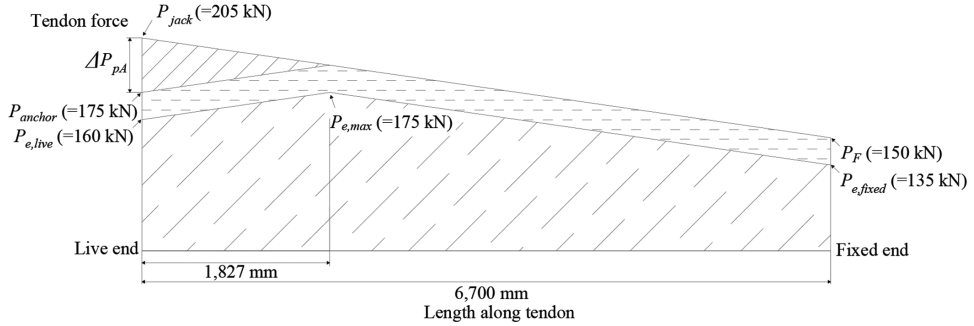

(c) Tendon tensile force along length at start of test (ACI 423.10R-16[44])

Fig. 14—Cracks and delamination, PT-induced equivalent forces, and tendon force distribution along length. (Note: 1 mm = 0.0394 in.; 1 kN = 0.2247 kip.)

a substantial effect. In Fig. 15, slabs ruptured when the deflection rate ceased vibrating along the reference point (zero point) and when peak points of amplitude gradually increased from that prior. These patterns were most obvious in tendon configurations of G- and S-types, which were encased in HDPE sheathing. Although the U-type, with no HDPE sheathing, experienced numerous extensive vibrations from the start of the fire test due to propagation of cracks, spalling, and delamination, the G- and S-types neglected minor influences with less fluctuation but reported significant structural damage at the end stage. Although the methodology for determining the deflection rate of each PT structure with HDPE sheathing when subjected to fire requires further investigation, justification for its use in unbonded tendon systems is shown.

CONCLUSIONS

In this study, the thermal and flexural behaviors of six post-tensioned (PT) concrete slabs with three different tendon configurations were evaluated by fire tests. To evaluate the fire-resistance performance of each PT slab, temperature variation at the bottom surface of the concrete slab and tendon, along with deflection and tendon tensile forces, was continuously recorded during said tests. Cracks, spalling, and delamination were investigated, and influential factors discussed. Based on the fire test results, the following conclusions were drawn:

1. Influencing factors for the change in stage from the initial plateau stage to the rapid temperature stage were the presence of galvanized steel ducts and high-density polyethylene (HDPE) sheathing. These elements provided increased thermal resistance at the surface interface, which delayed the increase in initial temperature, to the benefit of the structure in regard to fire-resistance performance.

2. Cover thickness significantly affected the fire-resistance performance of PT concrete slabs. G- and S-type fire endurance times increased by 36 and 125%, respectively, while U-type decreased by as much as 32%. By increasing concrete cover thickness of the slabs, heat transfer time from the bottom of the slab to the tendon also increased, which lessened fire damage. However, severe concrete cracks and fracture showed in the U-type, resulting in reduced fire endurance time. In the fire tests, increased cover thickness enhanced fire-resistance performance by relieving the generation of unpredicted damage to the tendon and structure, but in the case of the U-type, the need for crack control was evident.

3. Tendon tensile force measurements conducted during the fire tests revealed minor differences in degree and fluctuation between tendon configurations. Each configuration underwent three stages: increasing, decreasing, and rupture. Slab deflection and heat-degraded mechanical properties were influential factors.

4. Fire tests revealed three types of cracking (thermal shrinkage, flexural, and delamination) along with concrete

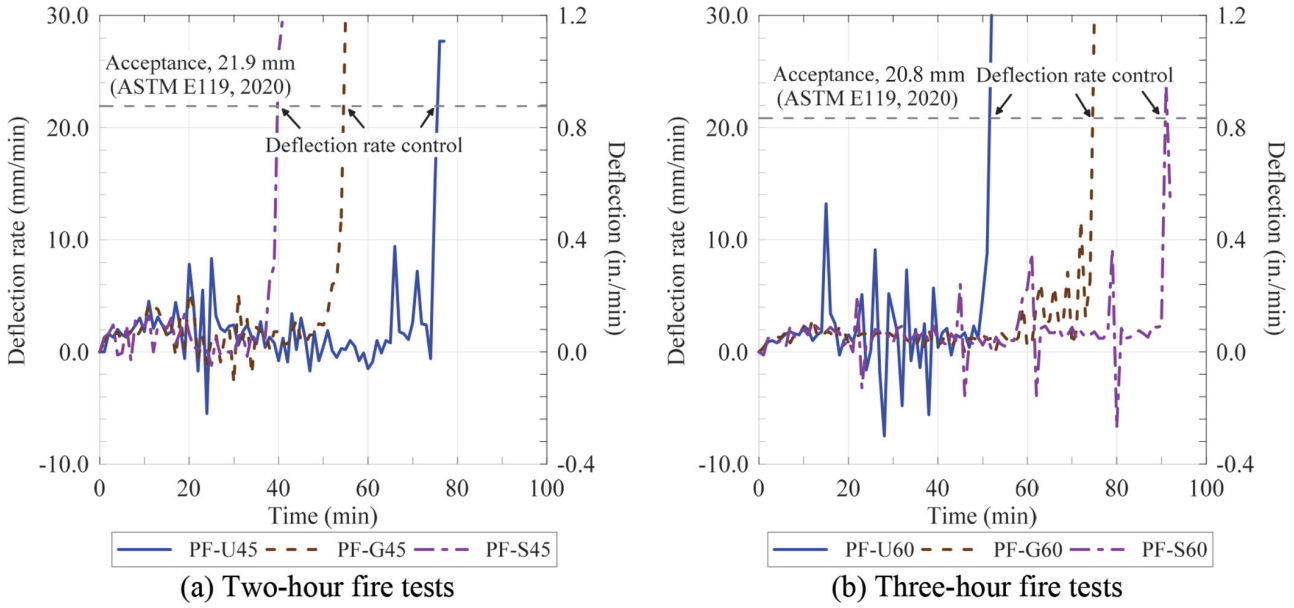

(a) Two-hour fire tests

(b) Three-hour fire tests

Fig. 15—Time-deflection rate curves at midspan of slabs.

delamination just outside anchorage zones, which had a substantial effect on the fire-resistance performance of the slabs. The tendon profile (negative parabola), applied tensile force, and tensile strength degradation all had an effect on concrete delamination, with maximum damaged depth due to delamination being 260 mm (10.2 in.), which equates to 93% of the original slab thickness. This would have been prevented if long tendons spanning multiple bays had been used, which is typical in practice, and much smaller increments in strain and/or transverse reinforcement had been used for the negative tendon curvature region just outside the reinforced anchorage zone.

As a future work, based on the experimental data, numerical studies are expected to be performed for analyzing the tendon tensile force variation and concrete delamination.

AUTHOR BIOS

ACI member **Siyoung Park** *is a former MS Student of structural engineering at Seoul National University, Seoul, South Korea, where he received his BS and MS. His research interests include the design and behavior of reinforced, prestressed, and post-tensioned concrete structures.*

Thomas H.-K. Kang, *FACI, is a Professor of structural engineering and interdisciplinary artificial intelligence at Seoul National University. He is a member of Joint ACI-PTI Committee 320, Post-Tensioned Structural Concrete Code; Joint ACI-ASCE Committees 352, Joints and Connections in Monolithic Concrete Structures, and 423, Prestressed Concrete; Joint ACI-ASME Committee 359, Concrete Containments for Nuclear Reactors; and ACI Subcommittee 318-T, Post-Tensioned Concrete. His research interests include the design and behavior of reinforced, prestressed, and post-tensioned concrete structures.*

ACKNOWLEDGMENTS

This work was supported by the Nuclear Safety Research Program through the Korea Foundation of Nuclear Safety (KoFONS) using the financial resources granted by the Nuclear Safety and Security Commission (NSSC) of the Republic of Korea. (No. 2203024-0122-SB110). The authors would also like to appreciate partial support by the Institute of Construction and Environmental Engineering at Seoul National University.

NOTATION

d = distance between extreme fiber of beam in compression zone and extreme fiber of beam in tensile zone, mm (in.)
h_j = thermal contact conductance, W/m^2·K (Btu/h·ft^2·°F)
$k_{c,c}(\theta)$ = coefficient for decrease of compressive strength of concrete
$k_{c,E}(\theta)$ = coefficient for decrease of elastic modulus of concrete
$k_{c,t}(\theta)$ = coefficient for decrease of tensile strength of concrete
$k_{s,E}(\theta)$ = coefficient for decrease of elastic modulus of steel
$k_{s,p}(\theta)$ = coefficient for decrease of proportional limit of steel
$k_{s,y}(\theta)$ = coefficient for decrease of yield strength of steel
L_c = clear span of beam, mm (in.)
P_{anchor} = strand force at anchorage device after seating, MPa (ksi)
P_e = effective force in prestressing steel, MPa (ksi)
$P_{e,fixed}$ = effective force in prestressing steel at fixed end, MPa (ksi)
$P_{e,live}$ = effective force in prestressing steel at live end, MPa (ksi)
$P_{e,max}$ = maximum effective force in prestressing steel along tendon length, MPa (ksi)
P_F = jacking force in prestressing steel at fixed end after anchor set, MPa (ksi)
$P_{F,i}$ = immediate force in prestressing steel at fixed end after jacking, MPa (ksi)
P_{jack} = jacking force in prestressing steel at live end, MPa (ksi)
q = heat flux, W/m^2 (Btu/h·ft^2)
w_{down} = uniformly distributed downward force from tendon to concrete, kN/m (kip/in.)
w_{up} = uniformly distributed upward force from tendon to concrete, kN/m (kip/in.)
ΔP_{pA} = change in force due to anchor set, MPa (ksi)
ΔT = temperature drop across interface, °C (°F)

REFERENCES

1. PTI TAB.1-06, "Post-Tensioning Manual," sixth edition, Post-Tensioning Institute, Farmington Hills, MI, 2006, 254 pp.

2. Naaman, A. E., *Prestressed Concrete Analysis and Design: Fundamentals*, second edition, Techno Press 3000, Ann Arbor, MI, 2004.

3. Shin, H.; Kang, T. H.-K.; and Park, J.-H., "Grouted Extruded-Strand Tendons: Friction Coefficients and Differential Individual Strand Forces," *ACI Structural Journal*, V. 117, No. 3, May 2020, pp. 223-233.

4. VSL, "VSL Strand Post-Tensioning Systems," VSL International Ltd., Köniz, Switzerland, 2015, 41 pp.

5. Park, S., "Fire Behavior of Post-Tensioned Concrete One-Way Members with Different Tendon Configuration," MS thesis, Seoul National University, Seoul, South Korea, 2022.

6. NEA/CSNI/R(2015)5, "Bonded or Unbonded Technologies for Nuclear Reactor Prestressed Concrete Containments," Organization for Economic Co-operation and Development (OECD), Paris, France, 2015, 227 pp.

7. Aslani, F., and Bastami, M., "Constitutive Relationships for Normal- and High-Strength Concrete at Elevated Temperatures," *ACI Materials Journal*, V. 108, No. 4, July-Aug. 2011, pp. 355-364.

8. Chang, Y. F.; Chen, Y. H.; Sheu, M. S.; and Yao, G. C., "Residual Stress–Strain Relationship for Concrete after Exposure to High Temperatures," *Cement and Concrete Research*, V. 36, No. 10, Oct. 2006, pp. 1999-2005. doi: 10.1016/j.cemconres.2006.05.029

9. Kodur, V. K. R.; Wang, T. C.; and Cheng, F. P., "Predicting the Fire Resistance Behaviour of High Strength Concrete Columns," *Cement and Concrete Composites*, V. 26, No. 2, Feb. 2004, pp. 141-153. doi: 10.1016/S0958-9465(03)00089-1

10. Du, Y.; Peng, J.-Z.; Liew, J. Y. R.; and Li, G.-Q., "Mechanical Properties of High Tensile Steel Cables at Elevated Temperatures," *Construction and Building Materials*, V. 182, Sept. 2018, pp. 52-65. doi: 10.1016/j.conbuildmat.2018.06.012

11. Kodur, V.; Dwaikat, M.; and Fike, R., "High-Temperature Properties of Steel for Fire Resistance Modeling of Structures," *Journal of Materials in Civil Engineering*, ASCE, V. 22, No. 5, May 2010, pp. 423-434. doi: 10.1061/(ASCE)MT.1943-5533.0000041

12. ASCE Committee on Fire Protection, "Structural Fire Protection," T. T. Lie, ed., ASCE Manual of Practice No. 78, American Society of Civil Engineers, Reston, VA, 1992.

13. BS EN 1992-1-2:2004, "Eurocode 2: Design of Concrete Structures – Part 1-2: General Rules – Structural Fire Design," European Committee for Standardization, Brussels, Belgium, 2004, 99 pp.

14. BS EN 1993-1-2:2005, "Eurocode 3: Design of Steel Structures – Part 1-2: General Rules – Structural Fire Design," European Committee for Standardization, Brussels, Belgium, 2005, 81 pp.

15. Zheng, W. Z.; Hou, X. M.; Shi, D. S.; and Xu, M. X., "Experimental Study on Concrete Spalling in Prestressed Slabs Subjected to Fire," *Fire Safety Journal*, V. 45, No. 5, Aug. 2010, pp. 283-297. doi: 10.1016/j.firesaf.2010.06.001

16. Dwaikat, M. B., and Kodur, V. K. R., "Fire Induced Spalling in High Strength Concrete Beams," *Fire Technology*, V. 46, No. 1, Jan. 2010, pp. 251-274. doi: 10.1007/s10694-009-0088-6

17. Kodur, V. K. R., "Spalling in High Strength Concrete Exposed to Fire: Concerns, Causes, Critical Parameters and Cures," *Advanced Technology in Structural Engineering: Proceedings of Structures Congress 2000*, M. Elgaaly, ed., Philadelphia, PA, 2000, pp. 1-9.

18. Sharma, U.; Zaidi, K.; and Bhandari, N., "Residual Compressive Stress-Strain Relationship for Concrete Subjected to Elevated Temperatures," *Journal of Structural Fire Engineering*, V. 3, No. 4, 2012, pp. 327-350. doi: 10.1260/2040-2317.3.4.327

19. Joint ACI-TMS Committee 216, "Code Requirements for Determining Fire Resistance of Concrete and Masonry Construction Assemblies (ACI/TMS 216.1-14) (Reapproved 2019)," American Concrete Institute, Farmington Hills, MI, 2014, 28 pp.

20. ICC, "2018 International Building Code (IBC)," International Code Council, Washington, DC, 2017.

21. Purkiss, J. A., and Li, L.-Y., *Fire Safety Engineering Design of Structures*, third edition, CRC Press, Boca Raton, FL, 2014, 454 pp.

22. Bailey, C. G., and Ellobody, E., "Fire Tests on Bonded Post-Tensioned Concrete Slabs," *Engineering Structures*, V. 31, No. 3, Mar. 2009, pp. 686-696. doi: 10.1016/j.engstruct.2008.11.009

23. Bailey, C. G., and Ellobody, E., "Fire Tests on Unbonded Post-Tensioned One-Way Concrete Slabs," *Magazine of Concrete Research*, V. 61, No. 1, Feb. 2009, pp. 67-76. doi: 10.1680/macr.2008.00005

24. Gales, J.; Bisby, L.; and Gillie, M., "Unbonded Post Tensioned Concrete Slabs in Fire – Part 1 – Experimental Response of Unbonded Tendons under Transient Localized Heating," *Journal of Structural Fire Engineering*, V. 2, No. 3, 2011, pp. 139-154. doi: 10.1260/2040-2317.2.3.139

25. MacLean, K. J. N., "Post-Fire Assessment of Unbonded Post-Tensioned Concrete Slabs: Strand Deterioration and Prestress Loss," MSc thesis, Queen's University, Kingston, ON, Canada, 2007, 200 pp.

26. Hou, X.; Zheng, W.; and Kodur, V. K. R., "Response of Unbonded Prestressed Concrete Continuous Slabs under Fire Exposure," *Engineering Structures*, V. 56, Nov. 2013, pp. 2139-2148. doi: 10.1016/j.engstruct.2013.08.035

27. Wosatko, A.; Pamin, J.; and Polak, M. A., "Application of Damage–Plasticity Models in Finite Element Analysis of Punching Shear," *Computers & Structures*, V. 151, Apr. 2015, pp. 73-85. doi: 10.1016/j.compstruc.2015.01.008

28. Genikomsou, A. S., and Polak, M. A., "Finite Element Analysis of Punching Shear of Concrete Slabs Using Damaged Plasticity Model in ABAQUS," *Engineering Structures*, V. 98, Sept. 2015, pp. 38-48. doi: 10.1016/j.engstruct.2015.04.016

29. Al Hamd, R. K. S.; Gillie, M.; Warren, H.; Torelli, G.; Stratford, T.; and Wang, Y., "The Effect of Load-Induced Thermal Strain on Flat Slab Behaviour at Elevated Temperatures," *Fire Safety Journal*, V. 97, Apr. 2018, pp. 12-18. doi: 10.1016/j.firesaf.2018.02.004

30. Kodur, V. K. R., and Bhatt, P. P., "A Numerical Approach for Modeling Response of Fiber Reinforced Polymer Strengthened Concrete Slabs Exposed to Fire," *Composite Structures*, V. 187, 2018, pp. 226-240. doi: 10.1016/j.compstruct.2017.12.051

31. Karaki, G.; Hawileh, R. A.; and Kodur, V. K. R., "Probabilistic-Based Approach for Evaluating the Thermal Response of Concrete Slabs under Fire Loading," *Journal of Structural Engineering*, ASCE, V. 147, No. 7, July 2021, p. 04021084. doi: 10.1061/(ASCE)ST.1943-541X.0003039

32. New Zealand Government, "Building Amendment Regulation 2012 – Schedule 1: The Building Code," Ministry of Business, Innovation and Employment, Wellington, New Zealand, 2012.

33. Yang, J. C.; Bundy, M.; Gross, J.; Hamins, A.; Sadek, F.; and Raghunathan, A., "International R&D Roadmap for Fire Resistance of Structures: Summary of NIST/CIB Workshop," NIST Special Publication 1188, National Institute of Standards and Technology, Gaithersburg, MD, 2015, 138 pp.

34. ASCE/SEI, "Performance-Based Structural Fire Design: Exemplar Designs of Four Regionally Diverse Buildings using ASCE 7-16, Appendix E," American Society of Civil Engineers, Reston, VA, 2020.

35. Dai, X.; Welch, S.; and Usmani, A., "A Critical Review of 'Travelling Fire' Scenarios for Performance-Based Structural Engineering," *Fire Safety Journal*, V. 91, July 2017, pp. 568-578. doi: 10.1016/j.firesaf.2017.04.001

36. Stern-Gottfried, J., and Rein, G., "Travelling Fires for Structural Design-Part II: Design Methodology," *Fire Safety Journal*, V. 54, Nov. 2012, pp. 96-112. doi: 10.1016/j.firesaf.2012.06.011

37. Jeanneret, C.; Gales, J.; Kotsovinos, P.; and Rein, G., "Acceptance Criteria for Unbonded Post-Tensioned Concrete Exposed to Travelling and Traditional Design Fires," *Fire Technology*, V. 56, No. 3, May 2020, pp. 1229-1252. doi: 10.1007/s10694-019-00927-4

38. Rackauskaite, E.; Hamel, C.; Law, A.; and Rein, G., "Improved Formulation of Travelling Fires and Application to Concrete and Steel Structures," *Structures*, V. 3, Aug. 2015, pp. 250-260. doi: 10.1016/j.istruc.2015.06.001

39. ACI Committee 318, "Building Code Requirements for Structural Concrete (ACI 318-19) and Commentary (ACI 318R-19) (Reapproved 2022)," American Concrete Institute, Farmington Hills, MI, 2019, 624 pp.

40. ASTM E119-20, "Standard Test Methods for Fire Tests of Building Construction and Materials," ASTM International, West Conshohocken, PA, 2020, 36 pp.

41. Lin, T. Y., "Load-Balancing Method for Design and Analysis of Prestressed Concrete Structures," *ACI Journal Proceedings*, V. 60, No. 6, June 1963, pp. 719-742.

42. ASTM C39/C39M-21, "Standard Test Method for Compressive Strength of Cylindrical Concrete Specimens," ASTM International, West Conshohocken, PA, 2021, 8 pp.

43. ISO 834-1:1999, "Fire-Resistance Tests — Elements of Building Construction — Part 1: General Requirements," International Organization for Standardization, Geneva, Switzerland, 1999, 25 pp.

44. Joint ACI-ASCE Committee 423, "Guide to Estimating Prestress Losses (ACI 423.10R-16)," American Concrete Institute, Farmington Hills, MI, 2016, 64 pp.

45. Cooper, M. G.; Mikic, B. B.; and Yovanovich, M. M., "Thermal Contact Conductance," *International Journal of Heat and Mass Transfer*, V. 12, No. 3, Mar. 1969, pp. 279-300. doi: 10.1016/0017-9310(69)90011-8

46. Yovanovich, M. M., "New Contact and Gap Conductance Correlations for Conforming Rough Surfaces," AIAA Paper No. 81-1164, AIAA 16th Thermophysics Conference, Palo Alto, CA, 1981, pp. 1-6.

47. Ghojel, J., "Experimental and Analytical Technique for Estimating Interface Thermal Conductance in Composite Structural Elements under Simulated Fire Conditions," *Experimental Thermal and Fluid Science*, V. 28, No. 4, Mar. 2004, pp. 347-354. doi: 10.1016/S0894-1777(03)00113-4

48. Ryan, J. V., and Robertson, A. F., "Proposed Criteria for Defining Load Failure of Beams, Floors, and Roof Constructions During Fire Tests," *Journal of Research of the National Bureau of Standards, Section C: Engineering and Instrumentation*, V. 63C, No. 2, Oct.-Dec. 1959, pp. 121-124. doi: 10.6028/jres.063C.017

NEW Symposium Publications from ACI

SP-347: Recent Developments in High Strain Rate Mechanics and Impact Behavior of Concrete

This Symposium Volume reports on the latest developments in the field of high-strain-rate mechanics and behavior of concrete subject to impact loads. This effort supports the mission of ACI Committee 370, Blast and Impact Load Effects, to develop and disseminate information on the design of concrete structures subjected to impact, as well as blast and other short-duration dynamic loads.

Available in PDF format: $69.50
(ACI members: $39.00) ($30.50 savings)

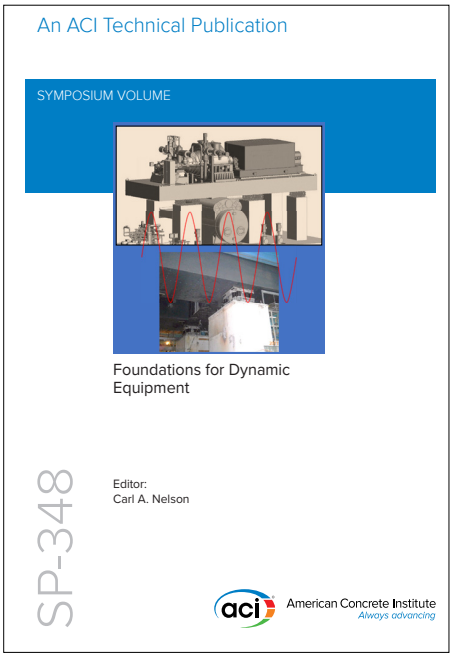

SP-348: Foundations for Dynamic Equipment

This special publication grew out of the Technical Session titled “Application of ACI 351-C Report on Dynamic Foundations,” held at the ACI Spring 2019 Convention in Québec City, Québec. Following this event, ACI Committee 351 decided to undertake a special publication with contributions from those session participants willing to develop their presentations into full-length papers. Three papers included in the current publication were contributed by these presenters and their coauthors, with six additional papers provided by others.

Available in PDF format: $69.50
(ACI members: $39.00) ($30.50 savings)

American Concrete Institute
+1.248.848.3700 • www.concrete.org